Scaling limit of the Ising model in a field

Uwe Grimm*
Institut für Physik, Technische Universität Chemnitz, D-09107 Chemnitz, Germany

Bernard Nienhuis†
Instituut voor Theoretische Fysica, Universiteit van Amsterdam, Valckenierstraat 65, 1018 XE Amsterdam, The Netherlands
(Received 30 September 1996)

The *dilute A_3 model* is a solvable interaction round a face model with three local states and adjacency conditions encoded by the Dynkin diagram of the Lie algebra A_3. It can be regarded as a solvable spin-1 Ising model at the critical temperature in a magnetic field. One therefore expects the scaling limit to be governed by Zamolodchikov's integrable perturbation of the $c=1/2$ conformal field theory. Indeed, a recent thermodynamic Bethe ansatz approach succeeded in unveiling the corresponding E_8 structure under certain assumptions on the nature of the Bethe ansatz solutions. In order to check these conjectures, we perform a detailed numerical investigation of the solutions of the Bethe ansatz equations for the critical and off-critical models. Scaling functions for the ground-state corrections and for the lowest spectral gaps are obtained, which give very precise numerical results for the lowest mass ratios in the massive scaling limit. While these agree perfectly with the E_8 mass ratios, we observe one state that seems to violate the assumptions underlying the thermodynamic Bethe ansatz calculation. We also analyze the critical spectrum of the dilute A_3 model, which exhibits excitations with a finite gap on top of the massless spectrum of the Ising conformal field theory. [S1063-651X(97)04204-9]

PACS number(s): 05.50.+q, 11.25.Hf, 75.10.Hk

I. INTRODUCTION

The Ising model [1] is, without doubt, one of the most frequently studied and best understood lattice models of classical statistical mechanics. Although Onsager's solution [2] of the two-dimensional (2D) Ising model without external field dates back half a century already, no analytic solution of the 2D Ising model in a magnetic field has been found.

However, the situation is somewhat different if considered from the viewpoint of field theory. The critical 2D Ising model corresponds to the $c=1/2$ conformal field theory (CFT) [3–6] of a massless Majorana fermion. It was Zamolodchikov [7–9] who noticed that a (symmetry-breaking) perturbation of this CFT with the relevant spin density operator [which has conformal dimensions $(\Delta,\bar{\Delta})=(1/16,\ 1/16)$] preserves infinitely many conservation laws and therefore leads to an integrable quantum field theory. The corresponding minimal theory contains eight massive particles with factorized (purely elastic) scattering [10–15]; the particle masses and the S-matrix elements are related to the exceptional Lie algebra E_8.

This integrable field theory describes an appropriate scaling limit of the 2D Ising model in a magnetic field. Numerically, the predictions for the lowest mass ratios have been verified by several authors [16–20]. As these results rely on relatively small size transfer matrix calculations or on Monte Carlo simulations, they provide rather crude checks for the lowest mass ratios only. Furthermore, the larger masses cannot be obtained directly as these lie above the two-particle threshold of the lightest particles and hence are buried in the continuum of scattering states. However, one can extract indirect information about the higher masses and the scattering amplitudes from the finite-size behavior of the lower masses [21,20]. Another, rather different, approach employs a truncated conformal Hilbert space [22,23], which, however, does not make the connection to the lattice model.

Similar theoretical and numerical investigations have also been performed for a variety of lattice models such as the eight-vertex model [24], the quantum Ising chain [16], the Lee-Yang model [22], the three-state Potts model [25], the tricritical Ising or the Blume-Capel model, respectively [26–28], the Ashkin-Teller model [29], the $Z(N)$ models [30], and the integrable restricted solid-on-solid models [31]. Recently, this has been extended to the study of form factors and correlation functions [32–37] and nonintegrable perturbations [38].

The discovery of a new class of lattice models [39–41] that are solvable in the presence of a symmetry-breaking field [40] has changed the situation considerably. Although we still cannot solve the 2D Ising model in a magnetic field, we now know a solvable model (the so-called dilute A_3 model) that belongs to the same universality class: it has a critical point of Ising type [40,42], and it is solvable in a symmetry-breaking field that corresponds to the spin density perturbation of the CFT [43]. Therefore, one expects this model to show the same properties in the scaling limit as the nonintegrable Ising model in a magnetic field. The dilute A_3 model is a spin-one Ising model (i.e., with three local states, say $s\in\{+1,0,-1\}$) with interactions between the four spins on the corners of an elementary square of the lattice.

The dilute A_L models are solvable by the Bethe ansatz (BA) [44,45]. By a thermodynamic Bethe ansatz (TBA) approach [44], the mass ratios and S matrix of the E_8 field theory have been obtained. However, this approach relies on assumptions on the nature of the BA solutions, which could

*Electronic address: u.grimm@physik.tu-chemnitz.de
†Electronic address: nienhuis@phys.uva.nl

not be substantiated by numerical solution of the BA equations (BAE) at criticality. Connections between the A_3 model and the exceptional Lie algebra E_8 are also revealed by the existence of corresponding Rogers-Ramanujan identities [46].

For our numerical investigation of the off-critical BAE, our main motivation was to check the assumptions on the conjectured string structure of the BA solutions. This could be achieved for the states with lowest masses, yielding at the same time very accurate numerical results not only for the mass ratios, but also for the complete scaling functions. However, we also found *one discrepancy* with the predictions of Ref. [44]. Within the range of scaling parameter values considered, the characteristic string type for a particle of mass m_4 does not match the proposed structure.

As a by-product of our investigation, we found that the critical spectrum also contains *massive* excitations besides the well-known conformal spectrum. This is one property that distinguishes the dilute A_3 model from the Ising model, which does not have such excitations. However, this does not contradict universality as that only concerns the universal properties of the systems in the vicinity of the critical point, which are the same for both models. The BA solutions corresponding to the massive excitations show the same type of strings as those conjectured for the massive scaling limit. Already for relatively small systems, these solutions lie very close to singularities of the BAE, which makes the numerical treatment difficult. Estimates of the corresponding mass ratios, which show no resemblance to the E_8 structure, are presented.

This paper is organized as follows. In Sec. II, the dilute A_3 model is introduced and the BAE are presented. The critical spectrum predicted by CFT and the behavior in the massive scaling limit are described. Furthermore, the assumptions about the form of the BA solutions formulated in Ref. [44] are summarized.

Section III contains the results of our numerical investigations. After a brief description of our numerical approach, we commence with the critical case, where not only are the scaling dimensions predicted by CFT considered, but also additional massive excitations in the spectrum are identified. Then, we show how the BA solutions behave as one goes away from criticality. Finally, we present our numerical scaling functions for the lowest gaps and the numerical results for the mass ratios in the massive scaling limit.

II. THE DILUTE A_3 MODEL

Because an immediate specialization to the A_3 case does not considerably simplify the equations, we keep the first part of this section on a more general level and consider the dilute A_L models. A detailed discussion of another member of this series, the dilute A_4 model, will be presented elsewhere [47].

The dilute A_L models are IRF (interaction round a face) models [48] of RSOS (restricted solid-on-solid) type [49] on the square lattice with adjacency conditions encoded by the Dynkin diagram of the Lie algebra A_L. In contrast to the usual (nondilute) RSOS models built on this adjacency graph (these are the Andrews-Baxter-Forrester models [49]), the effective adjacency graph of the dilute A_L model contains loops that connect each node to itself, see Fig. 1. In other words, one considers configurations of L local states or ''heights'' (labeled $1,2,\ldots,L$) on the vertices of the square lattice subject to the additional requirement that states on neighboring (adjacent) lattice sites may differ *at most* by 1. One then defines a statistical model by assigning Boltzmann weights to the elementary plaquettes (faces) of the lattice.

The face weights of the dilute A_L models are [40]

$$W\left(\begin{matrix} a & a \\ a & a \end{matrix}\middle| u\right) = \frac{\vartheta_1(6\lambda-u)\,\vartheta_1(3\lambda+u)}{\vartheta_1(6\lambda)\,\vartheta_1(3\lambda)} - \left(\frac{S_{a+1}}{S_a}\,\frac{\vartheta_4(2a\lambda-5\lambda)}{\vartheta_4(2a\lambda+\lambda)} + \frac{S_{a-1}}{S_a}\,\frac{\vartheta_4(2a\lambda+5\lambda)}{\vartheta_4(2a\lambda-\lambda)}\right)\frac{\vartheta_1(u)\,\vartheta_1(3\lambda-u)}{\vartheta_1(6\lambda)\,\vartheta_1(3\lambda)},$$

$$W\left(\begin{matrix} a\pm1 & a \\ a & a \end{matrix}\middle| u\right) = W\left(\begin{matrix} a & a \\ a & a\pm1 \end{matrix}\middle| u\right) = \frac{\vartheta_1(3\lambda-u)\,\vartheta_4(\pm2a\lambda+\lambda-u)}{\vartheta_1(3\lambda)\,\vartheta_4(\pm2a\lambda+\lambda)},$$

$$W\left(\begin{matrix} a & a \\ a\pm1 & a \end{matrix}\middle| u\right) = W\left(\begin{matrix} a & a\pm1 \\ a & a \end{matrix}\middle| u\right) = \left(\frac{S_{a\pm1}}{S_a}\right)^{1/2}\,\frac{\vartheta_1(u)\,\vartheta_4(\pm2a\lambda-2\lambda+u)}{\vartheta_1(3\lambda)\,\vartheta_4(\pm2a\lambda+\lambda)},$$

$$W\left(\begin{matrix} a & a\pm1 \\ a & a\pm1 \end{matrix}\middle| u\right) = W\left(\begin{matrix} a\pm1 & a\pm1 \\ a & a \end{matrix}\middle| u\right) = \left(\frac{\vartheta_4(\pm2a\lambda+3\lambda)\,\vartheta_4(\pm2a\lambda-\lambda)}{\vartheta_4^2(\pm2a\lambda+\lambda)}\right)^{1/2}\,\frac{\vartheta_1(u)\,\vartheta_1(3\lambda-u)}{\vartheta_1(2\lambda)\,\vartheta_1(3\lambda)},$$

$$W\left(\begin{matrix} a\pm1 & a \\ a & a\mp1 \end{matrix}\middle| u\right) = \frac{\vartheta_1(2\lambda-u)\,\vartheta_1(3\lambda-u)}{\vartheta_1(2\lambda)\,\vartheta_1(3\lambda)},$$

$$W\left(\begin{matrix} a & a\mp1 \\ a\pm1 & a \end{matrix}\middle| u\right) = -\left(\frac{S_{a-1}S_{a+1}}{S_a^2}\right)^{1/2}\,\frac{\vartheta_1(u)\,\vartheta_1(\lambda-u)}{\vartheta_1(2\lambda)\,\vartheta_1(3\lambda)},$$

$$W\left(\begin{matrix} a & a\pm1 \\ a\pm1 & a \end{matrix}\middle| u\right) = \frac{\vartheta_1(3\lambda-u)\,\vartheta_1(\pm4a\lambda+2\lambda+u)}{\vartheta_1(3\lambda)\,\vartheta_1(\pm4a\lambda+2\lambda)} + \frac{S_{a\pm1}}{S_a}\,\frac{\vartheta_1(u)\,\vartheta_1(\pm4a\lambda-\lambda+u)}{\vartheta_1(3\lambda)\,\vartheta_1(\pm4a\lambda+2\lambda)}$$

$$= \frac{\vartheta_1(3\lambda+u)\,\vartheta_1(\pm4a\lambda-4\lambda+u)}{\vartheta_1(3\lambda)\,\vartheta_1(\pm4a\lambda-4\lambda)} + \left(\frac{S_{a\mp1}}{S_a}\,\frac{\vartheta_1(4\lambda)}{\vartheta_1(2\lambda)} - \frac{\vartheta_4(\pm2a\lambda-5\lambda)}{\vartheta_4(\pm2a\lambda+\lambda)}\right)\frac{\vartheta_1(u)\,\vartheta_1(\pm4a\lambda-\lambda+u)}{\vartheta_1(3\lambda)\,\vartheta_1(\pm4a\lambda-4\lambda)}. \tag{2.1}$$

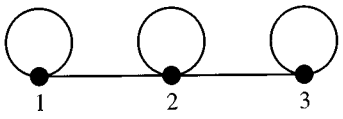

FIG. 1. Effective adjacency diagram of the dilute A_3 model.

Here, $a=1,2,\ldots,L$ labels the heights, and the possible values of the variable λ are determined by L [40]. The crossing factors S_a are given by

$$S_a=(-1)^a\frac{\vartheta_1(4a\lambda)}{\vartheta_4(2a\lambda)} \tag{2.2}$$

and $\vartheta_1(u)$, $\vartheta_4(u)$ are standard ϑ functions of nome q with $|q|<1$ [50]. These face weights satisfy the Yang-Baxter equation and therefore lead to an integrable lattice model. The corresponding row transfer matrices [48] for a fixed value of q form a one-parameter commuting family in the spectral parameter u.

In general, the dilute A_L models have four different branches for any value of L [40], distinguished by two possible values of λ with two regimes each for the spectral parameter u. Here, we are only interested in the dilute A_3 model ($L=3$) in a particular branch [40,42,44] where the model behaves like the Ising model in a magnetic field. For this case, $\lambda=5\pi/16$ and the spectral parameter u lies in the interval $0<u<3\lambda$, in which the Boltzmann weights (2.1) are positive. The spectral parameter controls the spatial anisotropy of the weights, with the isotropic point at $u=3\lambda/2$. The spin states $s\in\{+1,0,-1\}$ are given by $s=a-2$. It is the parameter q that acts like a magnetic field, breaking the $s\to -s$ symmetry; and the Ising critical point corresponds to $q=0$.

A. Bethe ansatz equations

The eigenvalues $\Lambda(u)$ of the row transfer matrix for a system of size N with periodic boundary conditions have the following form [44,45]:

$$\Lambda(u)=\omega^{\ell}\left(-\frac{\vartheta_1(u-2\lambda)\vartheta_1(u-3\lambda)}{\vartheta_1(2\lambda)\vartheta_1(3\lambda)}\right)^N\prod_{j=1}^{N}\frac{\vartheta_1(u-u_j+\lambda)}{\vartheta_1(u-u_j-\lambda)}+\left(-\frac{\vartheta_1(u)\vartheta_1(u-3\lambda)}{\vartheta_1(2\lambda)\vartheta_1(3\lambda)}\right)^N\prod_{j=1}^{N}\frac{\vartheta_1(u-u_j)\vartheta_1(u-u_j-3\lambda)}{\vartheta_1(u-u_j-\lambda)\vartheta_1(u-u_j-2\lambda)}$$
$$+\omega^{-\ell}\left(-\frac{\vartheta_1(u)\vartheta_1(u-\lambda)}{\vartheta_1(2\lambda)\vartheta_1(3\lambda)}\right)^N\prod_{j=1}^{N}\frac{\vartheta_1(u-u_j-4\lambda)}{\vartheta_1(u-u_j-2\lambda)}, \tag{2.3}$$

where $\omega=\exp[i\pi/(L+1)]$, and where the u_j, $j=1,\ldots,N$, form a solution of the set of N coupled BAE:

$$\omega^{\ell}\left(\frac{\vartheta_1(u_j-\lambda)}{\vartheta_1(u_j+\lambda)}\right)^N=-\prod_{k=1}^{N}\frac{\vartheta_1(u_j-u_k-2\lambda)\vartheta_1(u_j-u_k+\lambda)}{\vartheta_1(u_j-u_k+2\lambda)\vartheta_1(u_j-u_k-\lambda)}. \tag{2.4}$$

Here, $\ell=1,\ldots,L$ labels a sector related to the braid limit eigenvalues of the row transfer matrix at criticality ($q=0$). Whereas it is believed to be true that all eigenvalues of the transfer matrix are of the form (2.3), the converse is certainly wrong (at least off criticality) — the BAE (2.4) in general allow for many additional solutions that do not correspond to proper eigenvalues of the transfer matrix. For any numerically found solution of Eq. (2.4) one thus has to check whether it gives a proper eigenvalue of the transfer matrix (see Sec. III below).

The ϑ function $\vartheta_1(u)$ shows the (quasi) periodicity properties [50]

$$\vartheta_1(u+\pi)=-\vartheta_1(u)=\vartheta_1(-u), \tag{2.5a}$$

$$\vartheta_1(u+\pi\tau)=-\frac{1}{q}e^{-2iu}\vartheta_1(u) \tag{2.5b}$$

where $q=\exp(i\pi\tau)$ ($0<q<1$) with $\tau\in i\mathbb{R}$. Consider a solution $\{u_1,\ldots,u_N\}$ of the BAE (2.4) in sector ℓ. Clearly, nothing is changed if a multiple of π is added to any of the roots u_j.

More interesting is the result of adding $n\pi\tau$ ($n\in\mathbb{Z}$) to a root u_j. In this case, one obtains a solution of Eq. (2.4) with ω^{ℓ} replaced by $\exp(4ni\lambda)\omega^{\ell}$. Moreover, from Eq. (2.3) it is evident that these two solutions correspond to the same eigenvalue. This means that the ''sectors'' $\ell=1,\ldots,L$ lose their significance in the off-critical case ($q\neq 0$) since we can always adjust ℓ by adding or subtracting suitable multiples of $\pi\tau$ to some of the roots. Of course, this also yields many possibilities in which the phase factors cancel, and hence Eq. (2.4) is recovered without any alteration, which means that a single solution of the BAE can be presented in many ways differing by addition and subtraction of suitable multiples of $\pi\tau$ to some of the roots.

For the case of interest, it turns out that the largest eigenvalue $\Lambda_0(u)$ of the transfer matrix is given by a purely imaginary solution of the BAE (2.4) in the sector $\ell=1$. Therefore, in place of the roots u_j, we prefer to use $v_j=iu_j$ in what follows; thus the largest eigenvalue corresponds to a set of real BA roots v_j. General solutions to the BAE will, however, involve complex roots, which in the large-N limit typically arrange themselves into so-called *strings* (subsets of roots with approximately the same real part, in terms of the v_j). This is shown schematically in Fig.

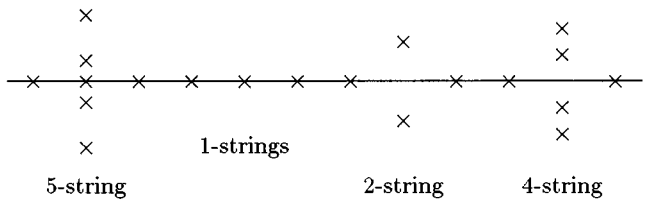

FIG. 2. Sketch of a typical arrangement of the Bethe ansatz roots v_j in the complex plane.

2, where the horizontal line represents the real axis. The unknowns u_j of the BAE are (up to a trivial transformation) the momenta of excitations (quasiparticles) relative to a specific eigenstate of the transfer matrix. The relation between momentum and the u_j is such that real values of v_j correspond to real momenta. Therefore the strings are complexes of quasiparticles with the same real part of the momentum, and can thus be viewed as bound states of quasiparticles. Note that the ''string content'' of a particular solution might well depend on the variable q, an example of this behavior will be given in Sec. III C below.

B. Conformal spectrum at criticality

The dilute A_3 model has a critical point of Ising type at $q=0$. Thus its critical limit (given by $q=0$, $N\to\infty$) is described by the $c=1/2$ CFT with scaling dimensions $\Delta \in \{0,\ 1/16,\ 1/2\}$. This has drastic consequences for the spectrum of the transfer matrix in the critical limit. Consider the scaled spectral gaps

$$x_j=\frac{N}{2\pi}\ln(\Lambda_0^{(0)}/\Lambda_j^{(0)}), \tag{2.6}$$

where $\Lambda_j^{(0)}$ are the eigenvalues of the transfer matrix with periodic boundary conditions at the isotropic point $u=3\lambda/2$, $\Lambda_0^{(0)}$ being the largest eigenvalue. In the critical limit, the spectrum of scaling dimensions x_j consists of ''conformal towers'' of states labeled by pairs $(\Delta+r,\bar{\Delta}+\bar{r})$ with scaled energy $x_j=\Delta+r+\bar{\Delta}+\bar{r}$, conformal spin $s_j=\Delta-\bar{\Delta}$, and momentum $p_j=r-\bar{r}$, where $r,\bar{r} \in \mathbb{N}_0$. They form representations of two commuting Virasoro algebras with central charge $c=1/2$. The degeneracies of the descendent states can be read off from the character functions of their irreducible representations with highest weight Δ. These can be written in the form [51]

$$\chi_0(z)=\sum_{n\in\mathbb{Z}} z^{4n^2+n}\Pi_V(z^2) =1+z^2+z^3+2z^4+2z^5+\cdots \tag{2.7a}$$

$$\chi_{1/2}(z)=\sum_{n\in\mathbb{Z}} z^{4n^2+3n+(1/2)}\Pi_V(z^2) =z^{1/2}(1+z+z^2+z^3+2z^4+\cdots) \tag{2.7b}$$

$$\chi_{1/16}(z)=z^{1/16}\prod_{m=1}^{\infty}(1+z^m) =z^{1/16}(1+z+z^2+2z^3+2z^4+\cdots), \tag{2.7c}$$

where $\Pi_V(z)$ is the generating function of the number of partitions

$$\Pi_V(z)=\prod_{m=1}^{\infty}\frac{1}{1-z^m}. \tag{2.8}$$

Moreover, the central charge $c=1/2$ manifests itself in the finite-size corrections of the largest eigenvalue [52]

$$-\ln(\Lambda_0^{(0)})=Nf_0+\frac{\pi c}{6N}+o(N^{-1}) \tag{2.9}$$

where f_0 denotes the bulk free energy for $u=3\lambda/2$.

C. Scaling limit

Taking into consideration the parameter q, one can approach the critical point by simultaneously performing the two limits $q\to 0$ and $N\to\infty$ keeping the scaling variable

$$\mu=qN^{15/8} \tag{2.10}$$

constant. Here, $\mu=0$ corresponds to the critical limit discussed above, and $\mu\to\infty$ gives the massive limit where Zamolodchikov's E_8 field theory results apply. In the scaling limit, the appropriately scaled spectral gaps

$$F_j=q^{-8/15}\ln(\Lambda_0/\Lambda_j) \tag{2.11}$$

become functions of the scaling variable μ alone. For the largest eigenvalue, we can also define a scaling function

$$F_0=q^{-8/15}[\ln(\Lambda_0)+Nf_0] \tag{2.12}$$

for the finite-size corrections of the largest eigenvalue, where $f_0=\lim_{N\to\infty}[-\ln(\Lambda_0)/N]$ is the bulk free energy again. Note that the face weights (2.1) for nome q and $-q$ are related by symmetry, thus it suffices to consider positive values of the nome.

In the massive limit ($\mu\to\infty$), the ratios

$$R_j=\frac{F_{j+1}}{F_1} \tag{2.13}$$

approach the particle mass ratios of the corresponding massive field theory. The masses of the eight stable particles are proportional to the entries of the Perron-Frobenius eigenvector of the Cartan matrix of the Lie algebra E_8, and their ratios (ordered by magnitude) are given by

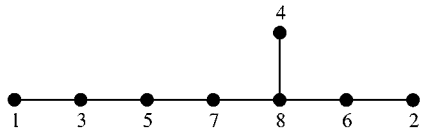

FIG. 3. The E_8 Dynkin diagram.

$$
\begin{aligned}
m_1/m &= 1, \\
m_2/m &= 2\cos(\pi/5) = 1.618\,034\cdots, \\
m_3/m &= 2\cos(\pi/30) = 1.989\,044\cdots, \\
m_4/m &= 4\cos(\pi/5)\cos(7\pi/30) = 2.404\,867\cdots, \\
m_5/m &= 4\cos(\pi/5)\cos(2\pi/15) = 2.956\,295\cdots, \\
m_6/m &= 4\cos(\pi/5)\cos(\pi/30) = 3.218\,340\cdots, \\
m_7/m &= 8\cos^2(\pi/5)\cos(7\pi/30) = 3.891\,157\cdots, \\
m_8/m &= 8\cos^2(\pi/5)\cos(2\pi/15) = 4.783\,386\cdots,
\end{aligned}
\tag{2.14}
$$

where $m = m_1$ defines the mass scale. The Dynkin diagram of E_8 is shown in Fig. 3, where our labeling of nodes follows the ordering of the masses.

In the TBA calculation of Ref. [44], each of the corresponding eight massive particles is associated to a particular string in the BA solution. In addition, it is assumed that, apart from these eight strings and the one-strings forming the vacuum solutions, no other string types occur in thermodynamically relevant quantities. With these assumptions, the TBA equations imply that the hole-type excitations in the one-strings have vanishing density. The density of one-strings can be eliminated from the calculation, which finally leads to the 8×8 scattering matrix of the E_8 factorized scattering theory [44].

In Table I, the nine string types are given, labeled by $t = 0,1,\ldots,8$ in the order used in Ref. [44], which corresponds to the usual labeling of the E_8 Dynkin diagram rather than that used in Fig. 3. From the data of Table I, the string of type t consists of $n^{(t)}$ roots of the form

TABLE I. The nine thermodynamically significant string types of Ref. [44] and the corresponding masses.

Mass	t	$n^{(t)}$	$\varepsilon^{(t)}$	$\Delta^{(t)}/5$
0	0	1	0	(0)
m_1	1	2	1	(−1,1)
m_2	7	4	0	(−3,−1,1,3)
m_3	2	4	0	(−4,−2,2,4)
m_4	8	5	1	(−12,−8,0,8,12)
m_5	3	6	1	(−7,−5,−1,1,5,7)
m_6	6	7	1	(−14,−6,−2,0,2,6,14)
m_7	4	8	0	(−10,−8,−4,−2,2,4,8,10)
m_8	5	10	1	(−13,−11,−7,−5,−1,1,5,7,11,13)

$$
v_k^{(t)} = v^{(t)} + \frac{i\pi}{32}\left(\Delta_k^{(t)} + 16\,\varepsilon_k^{(t)}\right), \tag{2.15}
$$

where $v^{(t)}$ denotes the center of the string on the real line.

III. NUMERICAL RESULTS

For the numerical treatment of the BAE (2.4) we used a modified Newton method [53]. The calculations were performed in extended precision FORTRAN (with 16 byte real numbers) on an IBM workstation.

As a first step, we solved the BAE at criticality ($q = 0$) for small system size and compared the corresponding eigenvalues (2.3) to those obtained by direct diagonalization of the transfer matrix using high precision arithmetic. This also served as a test of the performance of our programs. In particular, the *complete* set of solutions corresponding to zero-momentum eigenstates of the transfer matrix for systems of size $N \leqslant 6$ was obtained. In this way, the structure of the solutions for the largest eigenvalues could be identified. These solutions were followed as a function of the elliptic nome q. The results of this analysis were then generalized to larger system size by looking for solutions of the same type that differ by additional real roots only.

Since we are mainly interested in the mass ratios in the scaling limit, we exclusively considered zero momentum states. For solutions of the BAE, the momentum is obtained from the eigenvalue $\Lambda(0)$ (2.3) at spectral parameter $u = 0$, where the transfer matrix reduces to a shift operator. The numerical data for the gaps are taken at the isotropic point $u = 3\lambda/2$.

Because we want to follow solutions for varying q, which means that we have to repeat the calculation for a large number of values of q, we limited ourselves to systems of size $N \leqslant 100$. However, in certain cases the numerical accuracy of the calculations becomes the major problem. This happens, for instance, for BA solutions that contain roots that are very close to singularities of the BAE, or for solutions where differences between roots (or their real parts) become extremely small. These situations typically show up if one considers large values of the elliptic nome q (where the meaning of ''large'' depends on the system size), but also for the massive excitations of the critical dilute A_3 model discussed in Sec. III B below. As far as we can see, there are only two ways to go beyond the limitations imposed by these numerical problems; either by using higher precision arithmetic, or, to a lesser extent, by adjusting the program according to each specific type of BA solution (which we did to some extent by treating the ubiquitous complex conjugate pairs of BA roots with imaginary parts close to $\pm 11\pi/32$ in a special way).

A. Critical conformal spectrum

In the critical limit ($q = 0$, $N \to \infty$), the largest eigenvalues of the transfer matrix are organized according to the characters of representations of the Virasoro algebra with central charge $c = 1/2$ as described in Sec. II B above. Schematically, the resulting values for the scaling dimensions x in the zero-momentum sector and their distribution into the three sectors labeled by $\ell = 1,2,3$ are shown in Fig. 4.

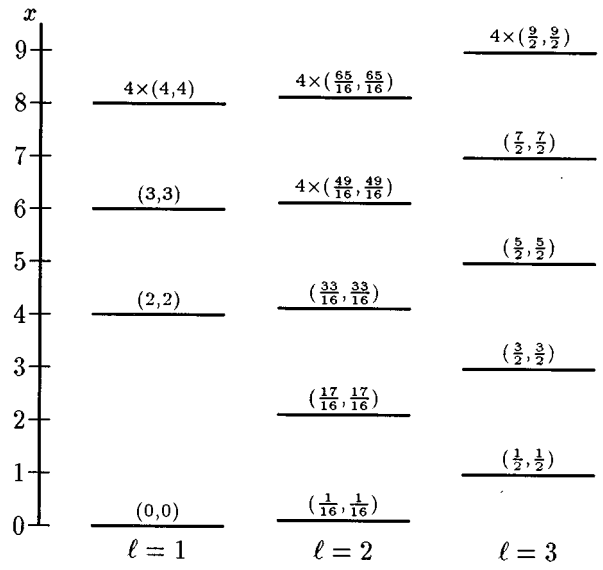

FIG. 4. Low-energy part of conformal zero-momentum spectrum for the critical dilute A_3 model.

In Table II, numerical values for the central charge and the lowest scaling dimensions obtained from the corresponding solutions of the BAE for systems of different sizes are presented. Here, Eq. (2.9) with the exact value of the bulk free energy [54,55] of the dilute A_3 model was used. All zero-momentum states with a critical scaling dimension of $x \leqslant 7$ have been found (compare Fig. 4), except one of the four excitations with conformal dimensions $(1/16+3, 1/16+3)$ for which, despite some effort, we have not been able to find the corresponding solution of the BAE. In particular, this includes all cases without degeneracy, i.e., where only a single zero-momentum state of a certain scaling dimension occurs in the conformal tower.

To keep the three remaining BA solutions with scaling dimension $x_9 = 6 + 1/8$ apart, we distinguish them by subscripts a, b, and c. Actually, it turns out that the two solutions denoted by b and c yield the same eigenvalue even for finite systems, which remains true also off criticality. Thus, we do not need to consider them separately unless we are interested in the BA solutions, which of course are different; see Sec. III C below.

While the numerical data are in perfect agreement with the exact values, it should be noted that the string structure of the critical BA solutions has no apparent similarity to those proposed in Ref. [44]. We shall come back to this point later.

B. Massive excitations at criticality

Analyzing the spectrum of largest eigenvalues of the transfer matrix, one observes that, in addition to the conformal spectrum discussed above, the spectrum contains *massive* excitations. More precisely, these are states with eigenvalues $\Lambda_k^{(0)}$ for which the quantities

$$y_k = \ln(\Lambda_0^{(0)}/\Lambda_k^{(0)}) \tag{3.1}$$

converge to a nonzero limit (mass) as $N \to \infty$; compare Eq. (2.6) for the conformal states where this limit gives zero.

Apparently, a number of different masses is involved, which are again characterized by particular strings in the BA solutions. Strikingly, the strings that we observed are among those listed in Table I. We have found explicit solutions containing strings of type $t = 1,\ 2,\ 3,\ 4$, and 7. In all cases, the roots forming these strings are — even for small systems — located extremely close to the singularity of the BAE, which they approach for $N \to \infty$. This requires a careful numerical treatment, and severely limits the system sizes we can treat. With the numerical accuracy of our program, we were able to get reliable results for systems of at most 20–30 sites, depending on the particular solution.

An example is given in Table III. Here, the solutions obtained by adding a number of ''massive'' two-strings $(t = 1)$ to the ground-state solution of a system of size $N = 4$ are presented. From the eigenvalues for larger systems, one can see that each additional ''massive'' two-string just adds the same mass, thus substantiating our interpretation in terms of massive particles.

Apparently, it is possible to add arbitrary numbers of these ''massive'' strings not only to the ground state, but to *each* solution corresponding to a conformal state. This means that the spectrum (at the critical point $q = 0$) contains infinitely many copies of the complete conformal spectrum, shifted with respect to the ground state by a mass determined by the collection of ''massive'' strings.

As to the observed ''massive'' strings, they fall into two classes: for $t = 1,\ 3$, and 7, we have a single solution of the BAE, whereas for $t = 2$ and 4 the solutions belong to eigenvalues that are doubly degenerate (for finite systems). Labeling the masses associated to the ''massive'' string type t by M_t, we obtain the numerical estimates

$$M_7/M_1 \approx 1.851\,86, \quad M_3/M_1 \approx 3.172\,13 \tag{3.2}$$

TABLE II. Finite-size approximants for central charge c and smallest scaling dimensions x_j.

N	c	x_1	x_2	x_3	x_4	x_5	x_6	x_7	x_8	x_{9a}	$x_{9b,c}$	x_{10}
10	0.499681	0.125080	1.014498	2.196	3.148	4.272	4.417	5.449	6.608	6.771	6.804	7.942
20	0.499920	0.125020	1.003543	2.142	3.034	4.062	4.191	5.098	6.142	6.274	6.274	7.196
50	0.499987	0.125003	1.000563	2.128	3.005	4.010	4.135	5.015	6.022	6.148	6.148	7.030
75	0.499994	0.125001	1.000250	2.126	3.002	4.004	4.130	5.007	6.010	6.135	6.135	7.013
100	0.499997	0.125001	1.000141	2.126	3.001	4.002	4.128	5.004	6.005	6.131	6.131	7.007
∞	1/2	1/8	1	$2+1/8$	3	4	$4+1/8$	5	6	$6+1/8$	$6+1/8$	7

TABLE III. Example of Bethe ansatz solutions at criticality in sector $\ell=1$, which differ from the ground-state solution for system size $N=4$ by a number of ''massive'' two-strings. Here, $\sigma=i\pi/32$.

$N=4$	$N=6$	$N=8$	$N=10$	$N=12$	$N=14$
1.977 471 499	1.980 014 437	1.982 321 219	1.984 408 860	1.986 312 526	1.988 062 914
0.575 364 766	0.577 361 036	0.579 176 248	0.580 821 977	0.582 324 931	0.583 708 690
−0.105 369 741	−0.105 850 465	−0.106 289 271	−0.106 688 316	−0.107 053 693	−0.107 390 875
−0.886 306 204	−0.888 679 105	−0.890 833 363	−0.892 784 131	−0.894 563 861	−0.896 200 997
	−0.000 000 072± 10.999 999 764σ	0.020 936 097± 10.999 999 615σ	0.035 854 325± 10.999 999 489σ	0.047 525 711± 10.999 999 373σ	0.057 153 974± 10.999 999 263σ
		−0.020 936 294± 10.999 999 730σ	−0.000 000 132± 10.999 999 570σ	0.014 769 565± 10.999 999 459σ	0.026 242 969± 10.999 999 320σ
			−0.035 854 556± 10.999 999 719σ	−0.014 769 869± 10.999 999 564σ	0.000 000 171± 10.999 999 444σ
				−0.047 525 969± 10.999 999 712σ	−0.026 243 304± 10.999 999 563σ
					−0.057 154 256± 10.999 999 706σ

and

$$M_2/M_1\approx 1.78, \quad M_4/M_1\approx 3.78 \tag{3.3}$$

for the ratios of the masses with respect to the smallest mass that is associated to the two-string ($t=1$). Note that these numbers are calculated from the eigenvalues of the transfer matrix with spectral parameter $u=3\lambda/2$.

This situation is similar to what is observed in the Hubbard model, where one has two types of excitations: so-called ''holons'' (carrying charge but no spin) and ''spinons'' (carrying spin but no charge) [56,57]. Generically, both excitations are massless, and the corresponding field theory consists of two coupled $c=1$ CFT. However, if the filling fraction (number of electrons per lattice site) is chosen to be precisely 1, the holons become massive while the spinons stay massless. At low energies, this theory is then described by a $c=1$ CFT with additional massive excitations [58].

C. Bethe ansatz roots off criticality

As mentioned above, the string structure of the BA roots at criticality does not seem to agree with the predictions of Ref. [44]. However, if one follows a particular solution as a function of the nome q, one finds that in many cases one encounters singularities of the BAE where the string structure changes.

The simplest example is given by the second largest eigenvalue, which corresponds to the conformal spin density field with dimensions $(1/16,\ 1/16)$ in the critical limit and to the lightest massive particle in the massive scaling limit. At criticality, the corresponding solution of the BAE differs from that of the largest eigenvalue (which contains real roots v_j only) by a single root with imaginary part $\pi/2$. However, as can been seen from Fig. 5, as q is increased from $q=0$, the complex root and one real root approach each other, until their real parts agree. At that point, the real parts of the two roots stay the same, but they move in the imaginary direction until they form a complex conjugate pair of roots (hence a two-string), which then persists for large values of q.

Comparing systems of different size, this mechanism always stays the same, the additional real roots just play the role of spectators. Moreover, the transition from one string type to another takes place at approximately the same value of the scaling parameter μ (2.10) as the system size is increased. More precisely, the scaling parameter values approach a nonzero limit as the system size tends to infinity. This implies that although $q\to 0$ in the scaling limit, for large values of μ (and in particular for the massive scaling limit $\mu\to\infty$), the two-string is the relevant type of solution.

The same scenario applies to the other excitations we considered. In Table IV, we compiled numerical values of the nonreal BA roots for systems of size $N=100$, both at criticality ($q=0$, i.e., $\mu=0$) and for a rather large value $\mu\approx 39.4$ of the scaling parameter (corresponding to $q=7/1000$ for $N=100$). Note that for $q\neq 0$ the real part of the roots v_j can be shifted by multiples of $-i\pi\tau=-\ln(q)\in\mathbb{R}_+$ $(0<q<1)$ as discussed in Sec. II A above. Using this property, we arranged the solutions such that the values of the nonreal roots have a real part in the interval $[0,-\ln(q)]$. Actually, as Table IV suggests, all nonreal roots are located in the vicinity of $-\ln(q)/2$ for sufficiently large scaling parameters μ. This also distinguishes these solutions from the ''massive'' strings at criticality considered above, whose centers are located close to the origin. Furthermore, the values of the nome q where changes in the string patterns for $N=100$ occur are also indicated in Table IV. All five single-particle states show at least one such point, whereas some of the two-particle states do not change as q is varied.

Although the relation between the scaling exponents on one end and the content of massive particles on the other is determined by the field theory, we are not aware that it has been calculated. Our results given in Table IV give an unambiguous connection for the lowest states, but they do not suggest an obvious pattern that can be generalized to the higher excitations.

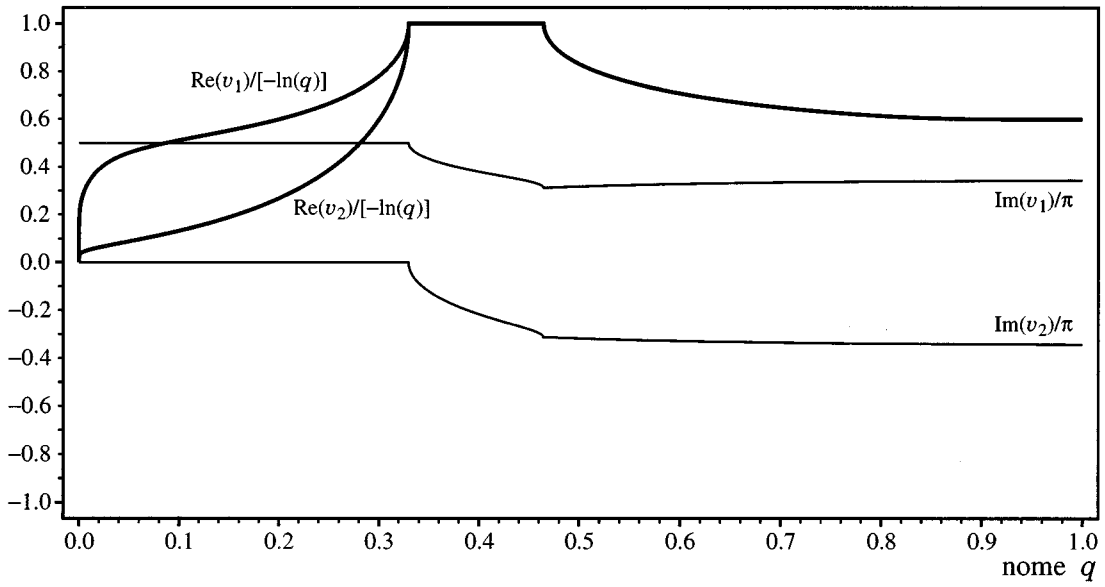

FIG. 5. Solution of BAE for the second largest eigenvalue for varying nome q. Thick lines denote the real parts [normalized by $-\ln(q)$] and thin lines the imaginary parts (in units of π) of the BA roots.

Comparing with the proposed string types of Ref. [44] given in Table I and by Eq. (2.15), one finds that the solutions for large scaling parameter agree with the predictions apart from the two states that contain a particle of mass m_4. Here, in place of a five-string with imaginary parts $\pm\pi/4$, $\pm 3\pi/8$, and $\pi/2$, the solution found numerically on first view looks more like a seven-string with imaginary parts $\pm\pi/32$, $\pm 7\pi/32$, $\pm 13\pi/32$, and $\pi/2$. However, in comparison to the other single-particle states, the real parts of the roots forming this ''string'' are quite far apart, which might be an indication of another change of pattern occurring at a larger value of q, which of course we cannot exclude on the basis of our numerical data.

Let us have a closer look at the single particle state with mass m_4. Figures 6 and 7 show the BA roots of the corresponding solutions for systems with $N=10$ and $N=20$ sites, respectively. For convenience, we plotted the real and imaginary parts of the roots, normalized by $-\ln(q)$ and by π as in Fig. 5, against $\mu^{8/15}=q^{8/15}N$. There are two obvious points (indicated by the arrows in Figs. 6 and 7) where nonanalyticities occur at approximately the same value of the scaling parameter for the two different sizes. These singularities are associated with the coincidence of two of the roots. However, Fig. 6 may suggest that another change will occur at a larger value of μ than numerically accessible by our routines, as the real parts of one real root and one of the two-strings approach each other. But, comparing with the same region of Fig. 7, no indication of this behavior remains, and the same holds true for the larger systems (up to $N=100$) that we examined. From this, we conclude that either there is no further change in the string pattern, or it has to occur for a very large value of the scaling parameter μ, which, however, seems rather unlikely to us.

Though this result is somewhat inconclusive, let us examine the string pattern of this solution in more detail. In particular, we are interested in the question of whether there are holes in the one-strings in this case. To see this, we consider the ''phase function''

$$\varphi(v)=\frac{1}{2\pi i}\ln\left[-\omega^{-\mathcal{N}}\left(\frac{\vartheta_1(iv+\lambda)}{\vartheta_1(iv-\lambda)}\right)^N \times\prod_{k=1}^{N}\frac{\vartheta_1(iv-iv_k-2\lambda)\,\vartheta_1(iv-iv_k+\lambda)}{\vartheta_1(iv-iv_k+2\lambda)\,\vartheta_1(iv-iv_k-\lambda)}\right], \tag{3.4}$$

which is basically the logarithm of the BAE (2.4), but now v_k denotes the roots of our particular BA solution, and we consider φ as a function of the complex variable v. By definition, $\varphi(v_j)\in\mathbb{Z}$ for all the roots v_j, $j=1,\ldots,N$. Restricted to real values of v, $\varphi(v)$ therefore takes integer values at all real solutions $v=v_j\in\mathbb{R}$, hence for all one-strings.

Figure 8 shows $\varphi(v)$ for the solution under consideration. Here, the size of the system is $N=20$, and $q=1/5$. The horizontal lines are drawn at integer values [the precise numbers are not relevant as they depend on the choice of branch in Eq. (3.4)], and the crosses located on intersections of these lines with the graph of $\varphi(v)$ denote the position of the real roots. The vertical lines are placed at the real parts of the remaining seven nonreal roots. As observed above, the single root with imaginary part $\pi/2$ lies somewhat separated from the three complex conjugate pairs, which are very close together (such that the three vertical lines appear as one thicker line in the figure). Moreover, the location of this single root coincides *precisely* with a hole in the one-strings, which may seem to disagree with the findings of Ref. [44]. However, the behavior of the roots as a function of parameters like q suggests that the roots with imaginary part $\pi/2$ are simply an alternative locus of the one-string.

On the basis of the numerical data, it thus seems that the

TABLE IV. Numerically observed string solutions for systems of size $N=100$ for nome $q=0$ ($\mu=0$) and $q=7/1000$ ($\mu\approx 39.4$). Only the values of the nonreal roots v_j are given. Here, $\varrho=-\ln(q)=-i\pi\tau$ and $\sigma=i\pi/32$. For those roots whose real part is very close to $\varrho/2$ or whose imaginary part is almost an integer times σ, such that the number of digits given is not sufficient to see the slight differences, the superscripts $+$ and $-$ indicate on which side the actual data lie. We also include ranges of q values within which changes of the string patterns are observed. The three solutions that correspond to a critical scaling dimension of $6+1/8$ are labeled by subscripts a, b, and c, where the latter two yield identical eigenvalues for finite systems.

$(\Delta+r,\Delta+r)$	Mass	Nonreal roots at $q=0$	Nonreal roots at $q=7/1000$	Pattern change
(0,0)	0			
$(\frac{1}{16},\frac{1}{16})$	m_1	$5.277\,011+16\,\sigma$	$0.500\,000^{+}\varrho\pm 11.000\,000^{-}\sigma$	0.000 138–0.000 139
				0.000 161–0.000 170
$(\frac{1}{2},\frac{1}{2})$	m_2	$-4.123\,856\pm 7.024\,170\sigma$	$0.500\,000^{-}\varrho\pm 4.999\,988\sigma$	0.000 560–0.000 640
		$-4.052\,796+16\,\sigma$	$0.500\,000^{-}\varrho\pm 15.000\,012\sigma$	
$(\frac{1}{16}+1,\frac{1}{16}+1)$	m_3	$-3.791\,098+16\,\sigma$	$0.500\,000^{+}\varrho\pm 12.011\,549\sigma$	0.000 440–0.000 450
		$3.719\,808\pm 11.045\,724\sigma$	$0.500\,000^{+}\varrho\pm 9.988\,451\sigma$	0.000 580–0.000 640
$(\frac{1}{2}+1,\frac{1}{2}+1)$	m_4	$-3.517\,907\pm 14.671\,118\sigma$	$0.485\,956\varrho\pm 0.992\,132\sigma$	0.000 340–0.000 350
		$-3.458\,496\pm 5.430\,532\sigma$	$0.486\,904\varrho\pm 7.000\,002\sigma$	0.002 900–0.002 950
		$3.981\,241+16\,\sigma$	$0.486\,904\varrho\pm 12.999\,998\sigma$	
			$0.500\,000^{+}\varrho+16\,\sigma$	
(2,2)	$2\,m_1$	$-3.245\,499\pm 10.982\,954\sigma$	$0.482\,282\varrho\pm 11.000\,000^{-}\sigma$	
		$3.237\,651\pm 10.937\,395\sigma$	$0.517\,718\varrho\pm 11.000\,000^{-}\sigma$	
$(\frac{1}{16}+2,\frac{1}{16}+2)$	m_1+m_2	$-3.282\,380\pm 10.815\,346\sigma$	$0.500\,000^{+}\varrho\pm 11.000\,000^{-}\sigma$	0.001 000–0.001 100
		$3.304\,607\pm 10.953\,718\sigma$	$0.500\,002\varrho\pm 15.000\,054\sigma$	0.001 410–0.001 420
		$4.238\,695+16\,\sigma$	$0.500\,002\varrho\pm 4.999\,946\sigma$	
$(\frac{1}{2}+2,\frac{1}{2}+2)$	m_5	$-3.356\,336\pm 12.564\,943\sigma$	$0.500\,000^{-}\varrho\pm 8.998\,677\sigma$	0.000 800–0.000 900
		$-3.326\,604\pm 8.981\,386\sigma$	$0.500\,000^{-}\varrho\pm 11.000\,000^{-}\sigma$	0.001 275–0.001 475
		$3.297\,948+16\,\sigma$	$0.500\,000^{-}\varrho\pm 13.001\,324\sigma$	
(3,3)	$2\,m_1$	$-2.875\,085\pm 11.000\,662\sigma$	$0.455\,576\varrho\pm 11.000\,000^{+}\sigma$	
		$2.875\,191\pm 11.000\,554\sigma$	$0.544\,424\varrho\pm 11.000\,000^{+}\sigma$	
$(\frac{1}{16}+3,\frac{1}{16}+3)_a$	m_1+m_3	$-2.890\,111\pm 11.001\,019\sigma$	$0.500\,000^{-}\varrho\pm 11.000\,000^{+}\sigma$	0.000 430–0.000 440
		$2.889\,954\pm 11.000\,849\sigma$	$0.500\,000^{+}\varrho\pm 11.928\,013\sigma$	0.000 520–0.000 550
		$4.741\,946+16\,\sigma$	$0.500\,000^{+}\varrho\pm 10.071\,987\sigma$	0.003 750–0.004 100
$(\frac{1}{16}+3,\frac{1}{16}+3)_b$	m_1+m_2	$-3.555\,509\pm 8.138\,452\sigma$	$0.471\,689\varrho\pm 11.000\,000^{+}\sigma$	0.000 370–0.000 380
		$-3.317\,682+16\,\sigma$	$0.517\,536\varrho\pm 5.000\,047\sigma$	
		$2.889\,954\pm 11.000\,849\sigma$	$0.517\,536\varrho\pm 14.999\,953\sigma$	
		$4.741\,946+16\,\sigma$		
$(\frac{1}{16}+3,\frac{1}{16}+3)_c$	m_1+m_2	$-2.890\,111\pm 11.001\,019\sigma$	$0.482\,461\varrho\pm 5.000\,047\sigma$	
		$3.091\,673\pm 5.267\,222\sigma$	$0.482\,461\varrho\pm 14.999\,953\sigma$	
		$3.097\,274\pm 14.605\,702\sigma$	$0.528\,311\varrho\pm 11.000\,000^{+}\sigma$	
$(\frac{1}{2}+3,\frac{1}{2}+3)$	m_1+m_4	$-3.447\,863\pm 6.844\,587\sigma$	$0.485\,373\varrho\pm 0.964\,059\sigma$	0.003 800–0.003 850
		$-3.399\,457+16\,\sigma$	$0.486\,904\varrho\pm 7.000\,017\sigma$	
		$-3.048\,514\pm 11.049\,729\sigma$	$0.486\,904\varrho\pm 12.999\,983\sigma$	
		$3.054\,397\pm 11.080\,356\sigma$	$0.500\,000^{+}\varrho\pm 11.000\,000^{+}\sigma$	
			$0.500\,000^{+}\varrho+16\,\sigma$	

string structure associated to the mass m_4 consists of the rather complicated pattern of a seven-string involving three complex conjugate pairs of roots (with imaginary parts $\pm\pi/32$, $\pm 7\pi/32$, and $\pm 13\pi/32$) and a neighboring root at $i\pi/2$, which comes together with a hole in the one-string distribution. Of course, in the infinite size limit the distance between the real parts of these roots becomes infinitesimal. It is not obvious what happens in the TBA calculation of Ref. [44] if their string type $t=8$ (see Table I) is replaced by the observed pattern, especially as we did not see the strings associated to the three largest masses. Nevertheless, we believe that the main ideas underlying the TBA treatment in Ref. [44] are correct, and that only details of the calculation would be affected.

Before we move on to a discussion of the scaling function, two short remarks regarding the BA solutions are in order. It should be noted that the ''massive'' strings mentioned previously in Sec. III B, which yield the massive excitations *at criticality*, do not undergo similar changes. These strings are always located very close to singularities of the

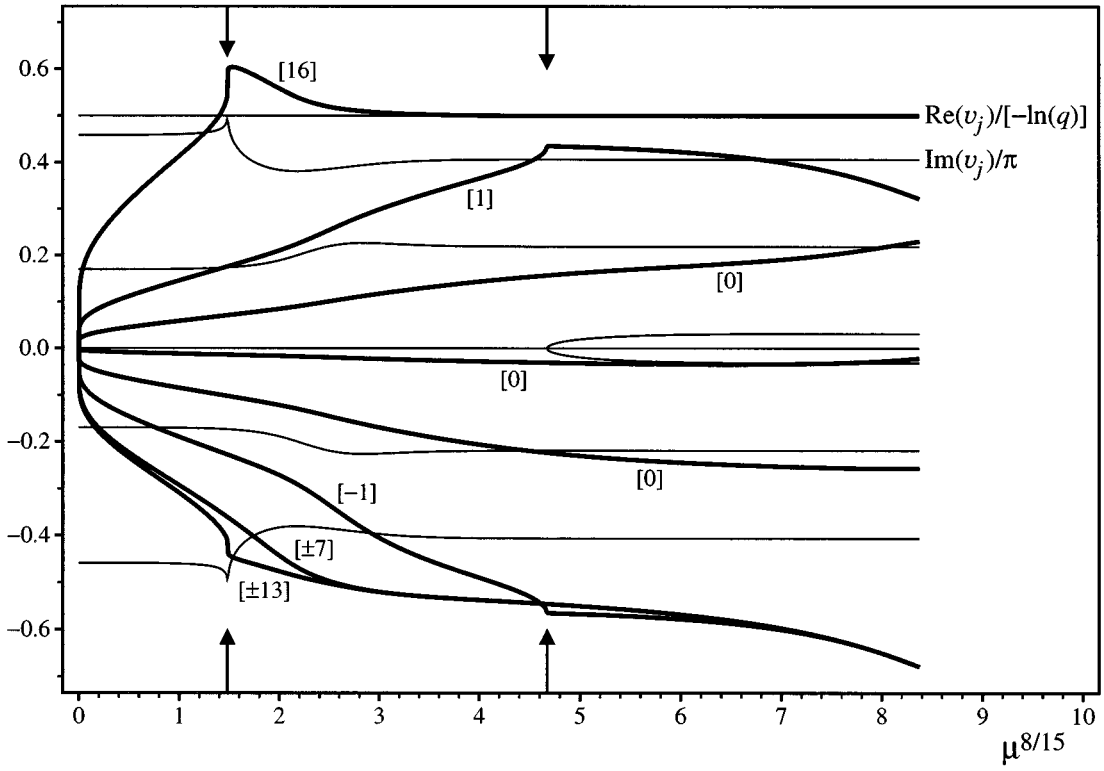

FIG. 6. Solution of BAE corresponding to the single-particle state with mass m_4 in the scaling limit. The system size is $N=10$. Thick lines denote the real parts [normalized by $-\ln(q)$] and thin lines the imaginary parts (in units of π) of the BA roots v_j. For each real part, the numbers in square brackets give the (approximate) imaginary parts (in units of $\pi/32$) for large values of the scaling parameter μ. The arrows indicate the positions of the singularities.

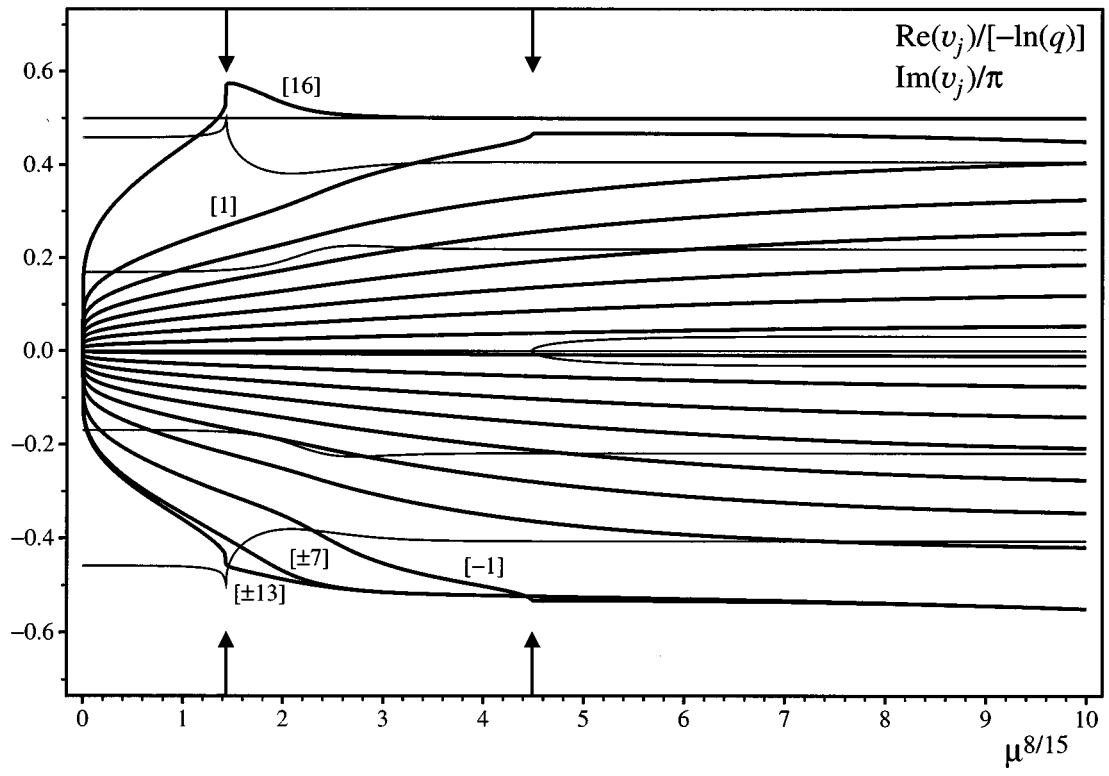

FIG. 7. Same as Fig. 6, but for system size $N=20$. For clarity, the numbers in square brackets have been omitted for all real roots.

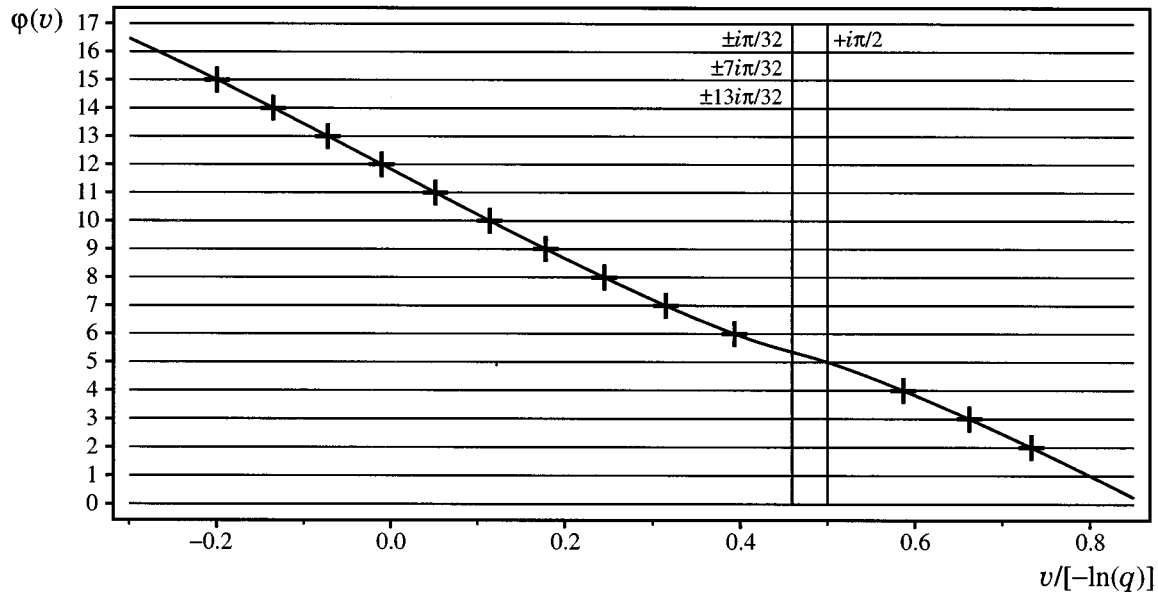

FIG. 8. The phase function $\varphi(v)$ [Eq. (3.4)] for the solution of BAE corresponding to the single-particle state with mass m_4 in the scaling limit. The system size is $N=20$, $q=1/5$. Horizontal lines are drawn at integer values, crosses at intersections with the graph of $\varphi(v)$ denote the real roots, and vertical lines indicate the positions of the real parts of the other seven roots.

BAE, and move even closer as the nome q is increased. Moreover, their centers lie at the origin (see e.g., Table III), whereas for the states belonging to the E_8 integrable field theory the strings cluster around the value $-\ln(q)/2$. Finally, let us mention that a similar behavior of BA roots has recently been observed in the solution of the XXZ Heisenberg chain, where the boundary twist acts as the varying parameter [59].

D. Scaling functions and mass ratios

Let us now turn to the results for the scaling functions $F_0(\mu)$ [Eq. (2.12)] and $F_j(\mu)$ [Eq. (2.11)]. For the latter, all zero-momentum states with a critical scaling dimension of $x\leqslant 7$ are considered, except the one missing excitation with conformal dimensions $(1/16+3,\ 1/16+3)$. In all cases, we use data from systems of size $N=50$, 75, and 100. For these

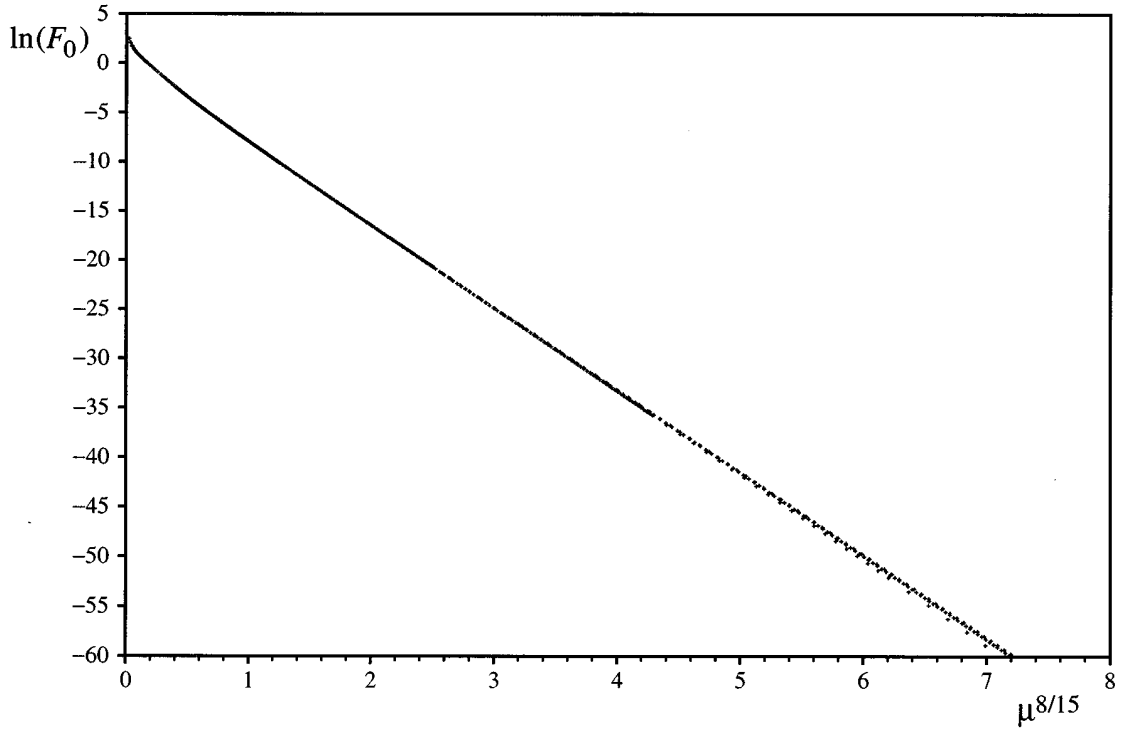

FIG. 9. Scaling function $F_0(\mu)$ [Eq. (2.12)] for the largest eigenvalue obtained from systems of size $N=50$, 75, and 100. Here, the logarithm of $F_0(\mu)$ is plotted against $\mu^{8/15}=q^{8/15}N$ [Eq. (2.10)].

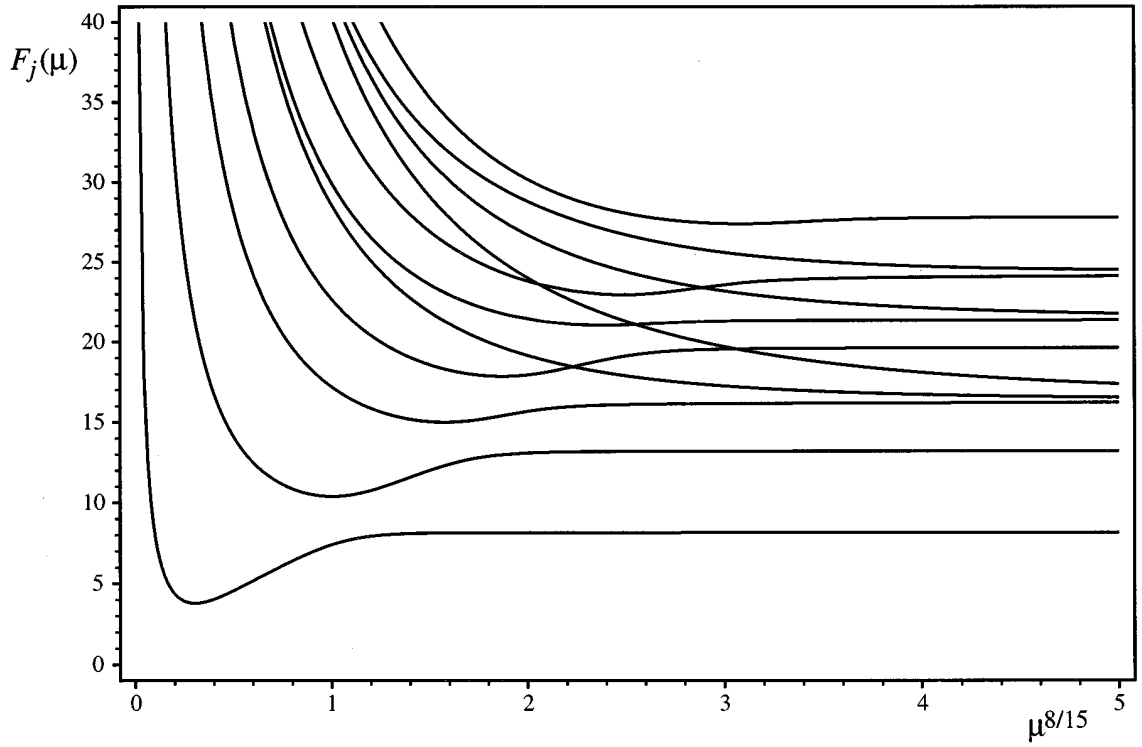

FIG. 10. Scaling functions $F_j(\mu)$ [Eq. (2.11)] for the excitations obtained from systems of size $N=100$.

sizes and the values of q we considered, it turns out that the corrections to scaling are so small that one can hardly recognize them in our figures.

In Fig. 9, the (natural) logarithm of $F_0(\mu)$ [which as defined in Eq. (2.12) is positive] is shown as a function of $\mu^{8/15}=q^{8/15}N$ [Eq. (2.10)]. Apart from the behavior for small q, the plot is nicely linear, showing the exponential decrease of F_0 as a function of $\mu^{8/15}$ down to about $\exp(-60)$ where the difference between the eigenvalues for the finite sizes and the bulk limit value becomes smaller than our numerical

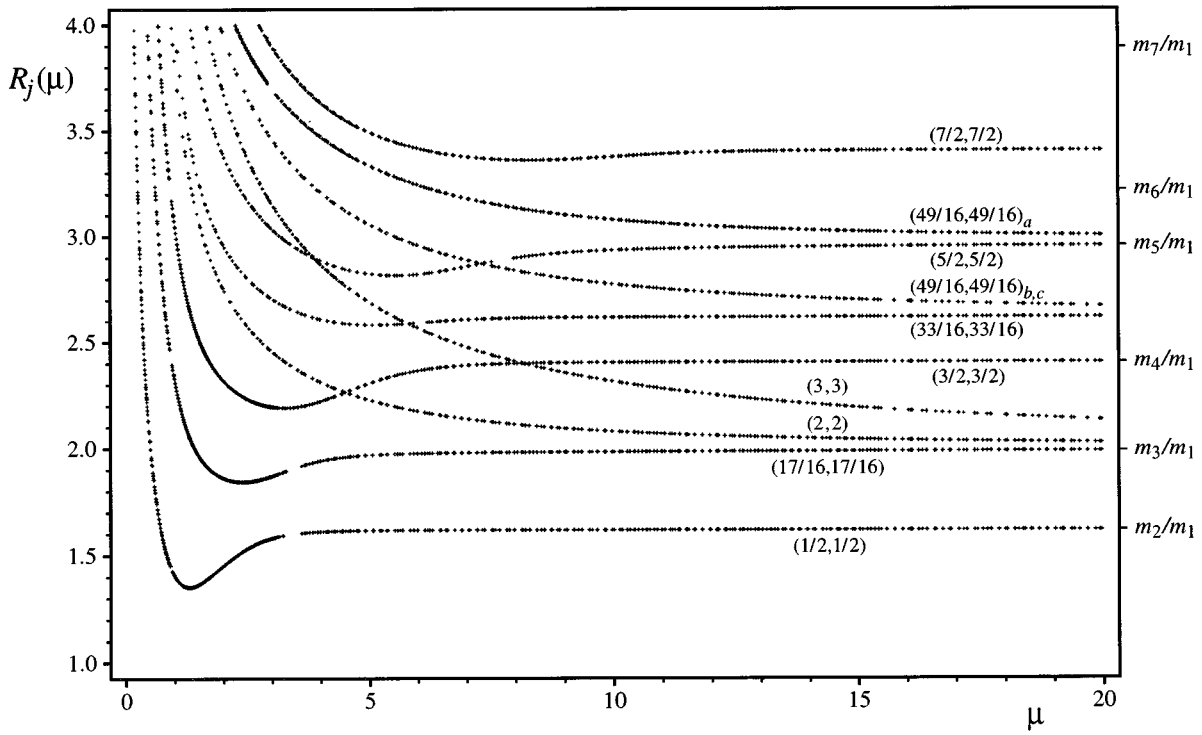

FIG. 11. Ratios of scaling functions $R_j(\mu)$ [Eq. (2.13)]. The individual data points shown stem from systems of size $N=50$, 75, and 100. Subscripts a, b, c distinguish different solutions with identical critical scaling dimensions. The E_8 mass ratios are indicated.

TABLE V. Ratios of scaled gaps for three values of the scaling parameter μ.

μ	N	R_1	R_2	R_3	R_4	R_5	R_6	R_7	R_{8a}	$R_{8b,c}$	R_9
	10	1.618 749	1.983 943	2.403 558	2.083 461	2.616 910	2.910 107	2.317 908	3.123 561	2.811 391	3.360 590
	20	1.618 037	1.983 923	2.403 649	2.081 017	2.617 335	2.930 942	2.320 478	3.086 893	2.781 193	3.369 241
10	50	1.618 024	1.983 977	2.403 797	2.079 804	2.617 468	2.934 096	2.314 580	3.078 762	2.773 762	3.375 544
	75	1.618 024	1.983 984	2.403 815	2.079 550	2.617 482	2.934 583	2.313 631	3.077 950	2.772 773	3.376 215
	100	1.618 025	1.983 990	2.403 834	2.079 551	2.617 497	2.934 617	2.313 523	3.077 537	2.772 605	3.376 509
	10	1.623 692	1.989 446	2.412 441	2.017 536	2.623 691	2.958 322	2.085 027	3.006 016	2.671 041	3.411 712
	20	1.618 144	1.987 688	2.405 009	2.025 316	2.618 144	2.954 218	2.129 306	3.006 016	2.669 638	3.404 917
20	50	1.618 034	1.987 597	2.404 866	2.026 212	2.618 034	2.954 289	2.132 554	3.003 342	2.669 034	3.404 805
	75	1.618 034	1.987 591	2.404 865	2.026 286	2.618 034	2.954 306	2.132 780	3.003 242	2.668 960	3.404 808
	100	1.618 034	1.987 589	2.404 865	2.026 315	2.618 034	2.954 311	2.132 871	3.003 212	2.668 941	3.404 808
	10	1.634 823	1.992 979	2.428 402	2.003 678	2.634 823	2.970 263	2.021 663	2.994 370	2.649 653	3.428 399
	20	1.618 424	1.988 671	2.405 376	2.012 146	2.618 424	2.956 329	2.071 838	2.992 915	2.644 399	3.405 376
30	50	1.618 036	1.988 497	2.404 869	2.013 483	2.618 036	2.956 009	2.078 248	2.992 952	2.645 130	3.404 869
	75	1.618 034	1.988 489	2.404 867	2.013 604	2.618 034	2.956 007	2.078 742	2.992 957	2.645 220	3.404 867
	100	1.618 034	1.988 486	2.404 867	2.013 644	2.618 034	2.956 007	2.078 950	2.992 958	2.645 248	3.404 867
∞	∞	1.618 034	1.989 044	2.404 867	2.000 000	2.618 034	2.956 295	2.000 000	2.989 044	2.618 034	3.404 867

precision, which also proves the performance of our numerical routines. Small deviations from scaling can be seen for larger values of q.

The scaling functions for the excitations $F_j(\mu)$ [Eq. (2.11)] are displayed in Fig. 10. The curves shown are piecewise linear plots connecting data points obtained from systems with $N=100$. For convenience, we again used $\mu^{8/15}=q^{8/15}N$ [Eq. (2.10)] on the horizontal axis. Qualitatively, the scaling functions agree with the results of previous numerical calculations for the Ising model in a magnetic field [17–19] and with the results of the truncated fermionic space approach; compare the figures given in Ref. [23]. The one-particle states can be recognized by their characteristic minima [17]. This becomes clearer when we consider their ratios $R_j(\mu)$ [Eq. (2.13)], which are presented in Fig. 11. Here, we again show individual data points that were obtained from systems of size $N=50$, 75, and 100, which obviously were large enough to keep corrections to scaling small. The ratios $R_j(\mu)$, given here against the scaling variable μ, are labeled by the corresponding conformal dimensions at criticality. We also indicated the single-particle mass ratios [Eq. (2.14)] of the E_8 field theory. Clearly, the agreement is convincing; more detail on the approach of the massive scaling limit is contained in Table V.

IV. CONCLUSIONS

The spectrum of the dilute A_3 model has been studied by numerical solution of the Bethe ansatz equations, both at and off criticality. This gives the correspondence between the lowest states of the conformal spectrum of the critical Ising model and those of the massive E_8 field theory (note that the connection given in Ref. [17] contains an obvious mistake).

At criticality, the spectrum consists for one part of massless excitations described by $c=1/2$ minimal CFT as in the critical Ising model, but in addition to these it contains massive excitations. Obviously, the masses of these excitations are linked to the appearance of particular strings in the Bethe ansatz solutions, which can be interpreted as massive particles. In our numerical analysis, we have seen at least five such ''massive'' strings. It is intriguing that all these strings (showing up in solutions *at criticality*) are among the conjectured list of ''thermodynamically significant string types'' in the TBA analysis [44] of the massive scaling limit. This is strongly suggestive of a connection between the Lie algebra E_8 and the masses of these excitations.

However, these are not the states that yield Zamolodchikov's E_8 field theory of the Ising model in a magnetic field. Those correspond to massless excitations at the critical point, which develop a mass due to the existence of the symmetry-breaking field. At criticality, the string structure of these states does not agree with the predictions of [44] — solving this puzzle had been the original motivation for this work. Our numerical results suggest a scenario that may solve this apparent contradiction: the string type of the relevant excitations undergoes a number of changes as the field is switched on, and for large systems these reorganizations take place at particular values of the scaling parameter μ. Therefore, the string structure entering the massive scaling limit $\mu\to\infty$ is that observed for large values of the elliptic nome q.

Numerically, we have been able to identify the single-particle states up to the fifth mass, and a number of two-particle states. Clearly, our results for the scaling functions are in complete agreement both with the analytic values of the mass ratios and with earlier numerical work on the Ising model in a magnetic field. As to the Bethe ansatz solutions, apart from one exception, the string structure for large field is that conjectured in [44]. The one exception concerns the string type associated to the particle of mass m_4. We found two states that contain this particle — one being the single-particle state with conformal dimensions (3/2, 3/2), the other a two-particle state that also contains the lightest particle and has scaling dimensions (7/2, 7/2) at criticality. In both cases, the observed string structures agree, but they differ from the one proposed in [44]; compare Table IV. Of

course, it cannot be ruled out completely that another change of string type appears at a larger value of the scaling parameter, but we found no trace of such behavior for scaling parameters up to $\mu \lesssim 80$. This clearly demands further clarification, and maybe the investigation of the dilute A_4 model can lead the way. In the scaling limit, this model is described by an E_7 theory of factorized scattering, but has so far eluded a TBA approach analogous to that of [44]. In this case, we have been able to identify *all* seven single-particle states and observed interesting string solutions, details will be published soon [47].

A number of interesting questions arise in connection with the massive excitations of the critical dilute A_3 model. This is one property of the dilute A_3 model that distinguishes it from the proper Ising model in a magnetic field, since the critical Ising model does not show such excitations. Moreover, we suppose that this phenomenon is not particular to the specific model and will show up in the other dilute models as well. It would be interesting to understand the physical nature of these excitations, and to obtain analytic predictions for the observed mass ratios. Also, their dispersion relations have not been studied because we concentrated on momentum zero states throughout this work.

Note added. — Recently we learned of the work of McCoy and Orrick [60]. From this we conclude that our massive excitations at criticality represent really the massless particles at a nonzero value of the momentum. That we see them in the zero-momentum sector as due to an extended Brillouin zone scheme, extending not from $-\pi$ to π but a multiple of that. This phenomenon had been observed before for the excitations of the antiferromagnetic three-state Potts quantum spin chain [61].

ACKNOWLEDGMENTS

U.G. gratefully acknowledges financial support of the Samenwerkingsverband FOM/SMC Mathematische Fysica during his stay in Amsterdam, where most of this work was done. The authors thank M. Baake, B. M. McCoy, P. A. Pearce, K. Schoutens, and S. O. Warnaar for interesting discussions and helpful comments.

[1] E. Ising, Z. Phys. **31**, 253 (1925).
[2] L. Onsager, Phys. Rev. **65**, 117 (1944).
[3] A. A. Belavin, A. M. Polyakov, and A. B. Zamolodchikov, Nucl. Phys. B **241**, 333 (1984).
[4] J. L. Cardy, in *Phase Transitions and Critical Phenomena*, edited by C. Domb and J. L. Lebowitz (Academic Press, London, 1987), Vol. 11, pp. 55–126.
[5] P. Ginsparg, in *Fields, Strings and Critical Phenomena*, Les Houches, Session XLIX, 1988, edited by E. Brézin and J. Zinn-Justin (Elsevier, Amsterdam, 1990), pp. 1–168.
[6] J. L. Cardy, in *Fields, Strings and Critical Phenomena* (Ref. [5]), pp. 169–245.
[7] A. B. Zamolodchikov, Pis'ma Zh. Éksp. Teor. Fiz. **46**, 129 (1987) [JETP Lett. **46**, 160 (1987)].
[8] A. B. Zamolodchikov, in *Integrable Systems in Quantum Field Theory and Statistical Mechanics*, Advanced Studies in Pure Mathematics Vol. 19, edited by M. Jimbo, T. Miwa, and A. Tsuchiya (Kinokuniya, Tokyo, 1989), pp. 641–647.
[9] A. B. Zamolodchikov, Int. J. Mod. Phys. A **4**, 4235 (1989).
[10] A. B. Zamolodchikov and Al. B. Zamolodchikov, Ann. Phys. (N.Y.) **120**, 253 (1979).
[11] R. Köberle and J. A. Swieca, Phys. Lett. **86B**, 209 (1979).
[12] E. Ogievetsky, N. Reshetikhin, and P. Wiegmann, Nucl. Phys. B **280**, 45 (1987).
[13] V. A. Fateev and A. B. Zamolodchikov, Int. J. Mod. Phys. A **5**, 1025 (1990).
[14] T. R. Klassen and E. Melzer, Nucl. Phys. B **338**, 485 (1990).
[15] G. Mussardo, Phys. Rep. **218**, 215 (1992).
[16] M. Henkel, J. Phys. A **20**, 995 (1987).
[17] I. R. Sagdeev and A. B. Zamolodchikov, Mod. Phys. Lett. B **3**, 1375 (1989).
[18] M. Henkel and H. Saleur, J. Phys. A **22**, L513 (1989).
[19] P. G. Lauwers and V. Rittenberg, Phys. Lett. B **233**, 197 (1989).
[20] M. Henkel, J. Phys. A **24**, L133 (1991).
[21] T. R. Klassen and E. Melzer, Nucl. Phys. B **362**, 329 (1991).
[22] V. P. Yurov and Al. B. Zamolodchikov, Int. J. Mod. Phys. A **5**, 3221 (1990).
[23] V. P. Yurov and Al. B. Zamolodchikov, Int. J. Mod. Phys. A **6**, 4556 (1991).
[24] M. T. Batchelor, M. N. Barber, and P. A. Pearce, J. Stat. Phys. **49**, 1117 (1987).
[25] A. B. Zamolodchikov, Int. J. Mod. Phys. A **3**, 743 (1988).
[26] M. Henkel, Phys. Lett. B **247**, 567 (1990).
[27] G. v. Gehlen, Nucl. Phys. B **330**, 741 (1990).
[28] M. Lässig, G. Mussardo, and J. L. Cardy, Nucl. Phys. B **348**, 591 (1991).
[29] M. Henkel and A. Ludwig, Phys. Lett. B **249**, 463 (1990).
[30] F. C. Alcaraz, J. Phys. A **23**, L1105 (1990).
[31] V. V. Bazhanov and N. Yu. Reshetikhin, Prog. Theor. Phys. Suppl. **102**, 301 (1990).
[32] G. Delfino and G. Mussardo, Nucl. Phys. B **455**, 724 (1995).
[33] R. Guida and N. Magnoli, Nucl. Phys. B **471**, 361 (1996).
[34] C. Acerbi, G. Mussardo and A. Valleriani, Int. J. Mod. Phys. A **11**, 5327 (1996).
[35] G. Delfino and P. Simonetti, Phys. Lett. B **383**, 450 (1996).
[36] G. Delfino, P. Simonetti, and J. L. Cardy, Phys. Lett. B **387**, 327 (1996).
[37] R. Guida and N. Magnoli, Nucl. Phys. B **483**, 563 (1997).
[38] G. Delfino, G. Mussardo, and P. Simonetti, Nucl. Phys. B **473**, 469 (1996).
[39] Ph. Roche, Phys. Lett. B **285**, 49 (1992).
[40] S. O. Warnaar, B. Nienhuis, and K. A. Seaton, Phys. Rev. Lett. **69**, 710 (1992).
[41] S. O. Warnaar and B. Nienhuis, J. Phys. A **26**, 2301 (1993).
[42] S. O. Warnaar, B. Nienhuis, and K. A. Seaton, Int. J. Mod. Phys. B **7**, 3727 (1993).
[43] S. O. Warnaar, P. A. Pearce, K. A. Seaton, and B. Nienhuis, J. Stat. Phys. **74**, 469 (1994).
[44] V. V. Bazhanov, B. Nienhuis, and S. O. Warnaar, Phys. Lett. B **322**, 198 (1994).

[45] Y. K. Zhou, P. A. Pearce, and U. Grimm, Physica A **222**, 261 (1995).
[46] S. O. Warnaar and P. A. Pearce, J. Phys. A **27**, L891 (1994).
[47] U. Grimm and B. Nienhuis (unpublished).
[48] R. J. Baxter, *Exactly Solved Models in Statistical Mechanics* (Academic Press, London, 1982).
[49] G. E. Andrews, R. J. Baxter, and P. J. Forrester, J. Stat. Phys. **35**, 193 (1984).
[50] I. S. Gradshteyn and I. M. Ryzhik, *Table of Integrals, Series and Products* (Academic Press, New York, 1965), pp. 926–933.
[51] M. Baake, J. Math. Phys. **29**, 1753 (1988).
[52] H. W. J. Blöte, J. L. Cardy, and M. P. Nightingale, Phys. Rev. Lett. **56**, 742 (1986).
[53] J. Stoer, *Einführung in die Numerische Mathematik I*, 2nd ed. (Springer, Berlin, 1976).
[54] S. O. Warnaar, M. T. Batchelor, and B. Nienhuis, J. Phys. A **25**, 3077 (1992).
[55] S. O. Warnaar, Ph.D. thesis, Universiteit van Amsterdam, 1993.
[56] A. Klümper, A. Schadschneider, and J. Zittartz, Z. Phys. B **78**, 99 (1990).
[57] F. H. L. Eβler and V. E. Korepin, Phys. Rev. Lett. **72**, 908 (1994).
[58] We thank K. Schoutens for making us aware of this similarity and for explaining the situation in the Hubbard model to us.
[59] N. Fumita, H. Itoyama, and T. Oota, Int. J. Mod. Phys. A (to be published).
[60] B. M. McCoy and W. P. Orrick, Phys. Lett. A (to be published).
[61] G. Albertini, S. Dasmahapatra, and B. M. McCoy, Phys. Lett. A **170**, 397 (1992).